Attosecond streaking in a nano-plasmonic field

2012 New J. Phys. 14 093034

(http://iopscience.iop.org/1367-2630/14/9/093034)

New Journal of Physics
The open-access journal for physics

Attosecond streaking in a nano-plasmonic field

F Kelkensberg[1], **A F Koenderink**[1] **and M J J Vrakking**[1,2,3]
[1] FOM Institute AMOLF, Science Park 104, 1098 XG, Amsterdam, The Netherlands
[2] Max-Born-Institut, Max-Born Strasse 2A, D-12489 Berlin, Germany
E-mail: Marc.Vrakking@mbi-berlin.de

New Journal of Physics **14** (2012) 093034 (19pp)
Received 8 January 2012
Published 18 September 2012
Online at http://www.njp.org/
doi:10.1088/1367-2630/14/9/093034

Abstract. A theoretical study of the application of attosecond streaking spectroscopy to time-resolved studies of the plasmonic fields surrounding isolated, resonantly excited spherical nanoparticles is presented. A classification of the different regimes in attosecond streaking is proposed and identified in our results that are derived from Mie calculations of plasmon fields, coupled to classical electron trajectory simulations. It is shown that in an attosecond streaking experiment, the electrons are almost exclusively sensitive to the component of the field parallel to the direction in which they are detected. This allows one to probe the different components of the field individually by resolving the angle of emission of the electrons. Finally, simulations based on fields calculated by finite-difference time-domain (FDTD) are compared with the results obtained using Mie fields. The two are found to be in good agreement with each other, supporting the notion that FDTD methods can be used to reliably investigate non-spherical structures.

[3] Author to whom any correspondence should be addressed.

Contents

1. Introduction

On the surface of a metal, evanescent waves can exist as a result of the interaction between electromagnetic fields and collective oscillations of the conduction electrons in the metal. These excitations are commonly referred to as surface plasmons and exist in a variety of forms. The electromagnetic fields follow from the solution of Maxwell's equations at the interface between a metal ($\epsilon < 0$) and a dielectric ($\epsilon > 0$). For a planar geometry, the solution leads to a traveling wave [1] with a corresponding dispersion curve that signifies the shorter wavelength of the surface plasmon compared to a free photon at a given frequency. The solution of Maxwell's equation for a spherical structure was first found by Mie [2]. The resulting theory has been highly successful in explaining the optical properties of metal and dielectric nanoparticles such as their scattering and absorption cross sections. The confinement of the surface plasmon wave on the sphere results in a resonance in the optical response of metal nanoparticles. The position of the resonance, largely determined by the permittivities of the metal and the surrounding medium, lies in the visible spectrum for metals such as silver and gold.

In recent years, interest in surface plasmons has grown, largely as a result of the increased control that is available in the fabrication of nano-structures. The increased control opens up possibilities to design components such as waveguides, mirrors and beamsplitters to manipulate surface plasmons on a chip on a scale much smaller than is possible for optical circuits [3]. Another important aspect of surface plasmons is the concentration of the electromagnetic wave, which leads to a higher field compared to a free-space electromagnetic wave. This field intensity enhancement, which can be up to a factor of 1000, is used in a variety of sensing applications of which surface-enhanced Raman spectroscopy (SERS) is the best-known example [4]. Nowadays, SERS is even possible at the single molecule level [5].

Resolving in space and time the underlying electron dynamics of plasmons would be the ultimate test for existing theoretical models and would therefore greatly help in understanding the physics. In particular, non-local effects, which cause deviations from the generic frequency-dependent dielectric function, are challenging current theoretical models [6–8]. However, in current experiments the electron dynamics are most of the time only indirectly observed. Time-resolved experiments are challenging because the fast timescales that are involved are at the limit of conventional laser pulses. Over the last decade, techniques based on autocorrelation [9–11], frequency-resolved optical gating (FROG) [12, 13] and spectral hole burning [14] have been developed to perform time-resolved measurements, each of them with its own advantages.

At the same time, a technique called attosecond streaking spectroscopy has been developed in attosecond science. In this technique, the dependence of the kinetic energy of electrons that are photoionized from an atom or molecule in the presence of a moderately strong (typical near-infrared (IR)) laser field is measured. With attosecond streaking spectroscopy, it is possible to perform a complete characterization of a light wave [15]. In earlier theoretical work, it has been realized that attosecond streaking could potentially also form the basis of a temporal characterization of a plasmonic field [16, 17]. An important advantage in the proposal of [16] is that in addition to the temporal resolution it is also possible to spatially resolve the fields with nanometer resolution by means of a photoemission electron microscope (PEEM). Moreover, the potential ability to resolve the absolute phase of the electric field, something that is not possible for any of the other methods, is an additional argument to develop attosecond streaking for plasmonic fields. In this paper, we present a theoretical investigation where we analyze the ability of attosecond streaking spectroscopy for determining the plasmonic fields that are created when small silver nano-spheres are resonantly excited using a moderately intense ultraviolet laser pulse. We show that measurements of photoelectrons that are ejected from the nanoparticle by an attosecond pulse are able to provide detailed information on the nature of the plasmon excitation and dephasing. In particular, we show that it is possible to probe the different components of the plasmon field individually by resolving the angle of emission of the electrons. We note that three theoretical studies have recently been published in which attosecond streaking is investigated as a tool to characterize plasmonic fields [18–20]. In the work by Skopalova *et al* [18], plasmonic fields in surface-deposited nano-structures are investigated in a specific structure in which a reconstruction of the localized field is shown to be possible, at least in idealized circumstances where the location of electron ejection is uniquely defined and when electrons are assumed to be selected with a very narrow detector acceptance angle. However, the paper only treats the situations that fulfil such ideal conditions. In the work of Süßmann *et al* [19], like in our work, the application of attosecond streaking to plasmonic fields surrounding spherical nanoparticles is considered. The main differences between our work and the work reported in [19] lies in the fact that we consider the case of a resonant plasmon excitation (as opposed to a non-resonant excitation in [19]) and in the methodology we use to study the streaking experiment, which in our case involves the application of both Mie theory and finite-difference time-domain (FDTD) methods. Finally, after this paper was submitted for publication, a new paper by Borisov *et al* [20] has been published, which calculates the attosecond streaking from rectangular nano-plasmonic antennas and from gas phase nanoparticles. These calculations were performed for a fixed photoelectron kinetic energy of 2 au and for photoelectron ejection along the common polarization direction of the IR laser and the ionizing attosecond pulses. Our work goes beyond this in that we also consider electron ejection in other directions and in that we explore the dependence of the streaking spectrograms on the kinetic energy of the ejected electrons, varying this energy between 20 eV and 1 keV, thereby changing between a regime where the electron leaves the plasmon field adiabatically to a regime where the electron leaves the plasmon field on a timescale that is short compared to the optical cycle.

2. Three regimes of attosecond streaking

In an attosecond streaking experiment, electrons are generated by photoionization with an attosecond pulse in the presence of a moderately strong IR field. Since the attosecond pulse

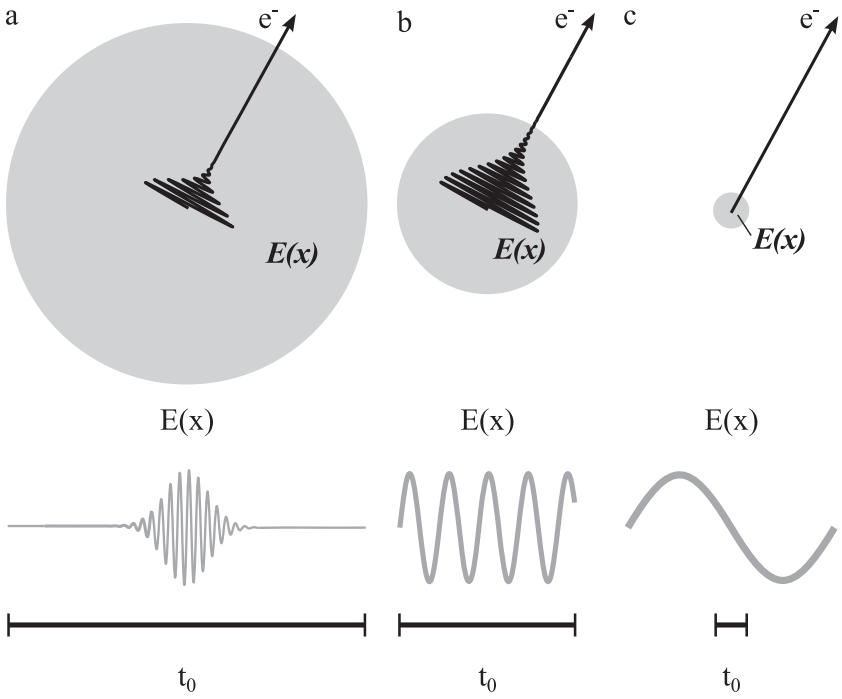

Figure 1. Three regimes of attosecond streaking can be distinguished by comparing the time t_0 it takes for an electron to leave the field to the pulse duration t_p and the period T of the field. In (a) ($t_0 \gg t_p$), the electron stays within the field from the time it is born to the end of the pulse. When $T \ll t_0 \ll t_p$ (b), the electron moves out of the field in a time that covers multiple optical cycles. In (c) ($t_0 \ll T$), the electron leaves the field 'instantaneously', i.e. within a fraction of an optical cycle.

is short compared to the period of the IR field, ionization takes place at a well-defined moment within that period. After the ionization the freed electrons interact with the IR field and thereby their momentum after this interaction is dependent on the moment of ionization. This time-to-momentum mapping allows characterization of the field by measuring the momentum (or energy) of the electrons. The outcome of an attosecond streaking experiment depends on whether or not the electron experiences a spatial variation of the field from the time it is born till it is detected. Three limiting situations are possible, based on the relation between the time it takes for an electron to leave the field (t_0), the period of the field T and the pulse duration t_p. The characteristic time t_0 is determined by the geometrical extension of the field r_0 and the velocity of the electron v_0 according to $t_0 = r_0/v_0$. In figure 1, a schematic representation of the three cases is given.

The first case (figure 1(a)) occurs when the laser pulse is short compared to the time it takes the electron to leave the field ($t_0 \gg t_p$). With such a short pulse the electron does not experience a spatial variation of the field and remains in the field from the time it is born to the end of the pulse. This is the situation generally encountered in attosecond streaking experiments in a laser field. A classical analysis of the interaction of the electron with the field in this case shows that the final momentum $\mathbf{p}_f$ is directly related to the vector potential

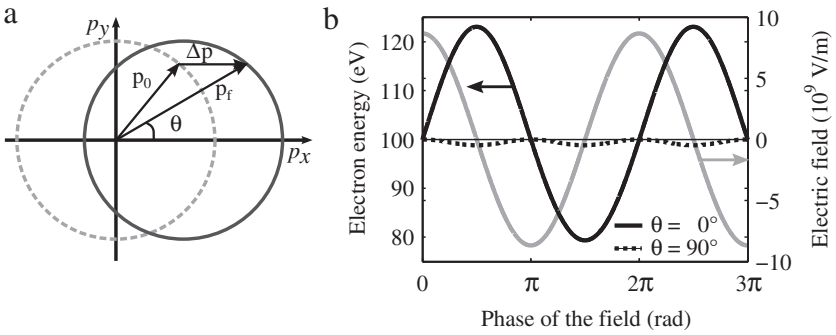

Figure 2. Principle of attosecond photoelectron streaking. (a) The dashed circle shows the momentum distribution in the xy plane produced by an attosecond pulse, which is subsequently shifted by $\Delta\mathbf{p}(t_i) = -e\mathbf{A}(\mathbf{t}_i)$ through interaction with the laser field. In (b) the resulting final energy $W_f(t_i)$ for $\theta = 0^\circ$ (solid black line) and for $\theta = 90^\circ$ (dotted black line) is plotted as a function of the phase of the laser field together with the laser field with a wavelength of 800 nm and an intensity of 10^{13} W cm^{-2}.

at the moment of ionization $\mathbf{A}_L(t_i)$ [21]:

$$\mathbf{p}_f = \mathbf{p}_0 - e\mathbf{A}_L(t_i), \tag{1}$$

where $\mathbf{p}_0$ is the initial momentum of the electron acquired in the ionization process that produces it. The momentum shift is schematically illustrated in figure 2(a) where an idealized momentum map of photoelectrons that are initially ejected uniformly in all directions is displayed. A linearly polarized laser field displaces the circle in the momentum map by an amount equal to $-e\mathbf{A}_L(t_i)$. The field is polarized in the x-direction and propagates along the z-axis, which is the convention adopted throughout this paper. The field-induced momentum displacement results in a photoelectron energy W_f that depends on t_i and on the observation angle θ between the direction of the velocity of the electron and the polarization axis [21]. When a laser field of $E(t) = E_0(t)\cos\omega_l t$ is assumed, the final energy of the electrons detected parallel ($\theta = 0^\circ$) and perpendicular ($\theta = 90^\circ$) to the laser polarization is given by[4]

$$W_f(t_i, \theta = 0^\circ) = W_0 + 2U_p \sin^2\omega_l t_i + \sqrt{8W_0U_p}\sin\omega_l t_i, \tag{2}$$

$$W_f(t_i, \theta = 90^\circ) = W_0 - 2U_p \sin^2\omega_l t_i \tag{3}$$

with ω_l being the frequency and $E_0(t)$ the envelope of the field. $W_0 = p_0^2/2m_e$ is the starting energy of the electron with mass m_e. U_p is the ponderomotive energy, which is given by $U_p = e^2E_0(t)^2/4m_e\omega_l^2$. This is the (cycle-averaged) energy connected with the quiver motion of the electron in the laser field. In figure 2(b) the final energy W_f described by equation (2) is plotted as a function of the phase of the laser field at the moment of ionization $\omega_l t_i$ (solid black line) together with the laser field (gray line). Figure 2(b) shows that electrons detected parallel to the laser polarization ($\theta = 0^\circ$) experience large positive and negative shifts in energy. The dotted black line in figure 2(b) shows the final energy for electrons detected perpendicular

[4] Equations (2) and (3) are valid for the situations in which the starting energy W_0 is much larger than the ponderomotive energy U_p, which is usually the case in attosecond streaking experiments.

to the laser polarization (equation (3)). These electrons experience energy shifts that are much smaller and only negative [22].

The assumption that the electron does not experience a spatial variation of the field before the field has turned off ($t_0 \gg t_p$) might not apply when attosecond streaking spectroscopy is applied to probe localized plasmon fields. In the second case (figure 1(b)), the electron can exit the field during the laser pulse but its exit takes many optical cycles ($T \ll t_0 \ll t_p$), i.e. the electron leaves the field adiabatically.

While this adiabatic situation is vastly different from the previous case, where the pulse dies out before the electron leaves the field (figure 1(a)), it only results in an additional (constant) offset of U_p in the final energy. This offset is the result of the ponderomotive force $\mathbf{F}_p = -\nabla_{\mathbf{r}} U_p(r)$ that the electron experiences while leaving the field, a phenomenon well known from above threshold ionization by long laser pulses [23]. Streaking in a continuous field with a finite size is thus described by (electron emission parallel to the polarization of the field)

$$W_f(t_i) = W_0 + U_p + 2U_p \sin^2 \omega_l t_i + \sqrt{8 W_0 U_p} \sin \omega_l t_i. \tag{4}$$

The offset is hardly significant since, in general, U_p will be small compared to the central energy and the energy width of the attosecond laser pulse that produces the electron.

The last case (figure 1(c)) occurs when the electron exits the field within a short period compared to the optical cycle ($t_0 \ll T$) and describes the situation that was considered in [16]. Provided that the field extension is sufficiently small and the initial kinetic energy is sufficiently large ($t_0 \ll T$), the electron can be assumed to leave the localized field 'instantaneously'. In such a situation the electron does not feel the oscillations of the field at all and the problem becomes (quasi-) electrostatic in nature. In the instantaneous limit the outcome of an attosecond streaking experiment is governed by the electrostatic scalar potential of the field $\Phi(t_i)$ ($\mathbf{E}(t) = -\nabla\Phi(t)$):

$$W_f(t_i) = W_0 + e\Phi(t_i). \tag{5}$$

In stark contrast to the two previous cases in which electron streaking reveals the vector potential, in this instantaneous picture the electron streaking curve will oscillate in phase with the electric field ($E(t)$). Another important difference is that the energy shift does not depend on the starting energy W_0 or angle of emission θ. Although there might be situations where the approximation $t_0 \ll T$ holds, specifically when the localized field is of the order of a few nanometers, in general there will be an intermediate regime where none of the approximations hold, i.e. when $t_0 \approx T$. The aim of this work is to bridge the gap between the different distinct limits and investigate theoretically whether it is possible to probe localized fields with attosecond pulses if one does not completely satisfy either one of the criteria discussed above.

From the above, it may be clear that attosecond streaking shows strong similarities to previous experiments and calculations on the ponderomotive acceleration of electrons by plasmon fields [24–26], which has recently been extended to few-cycle laser pulses [27–29]. In these experiments both ionization and excitation are performed by a single laser pulse, which makes it distinct from the present analysis. More specifically, in attosecond streaking the electron starts with a relatively high kinetic energy and the ponderomotive energy is small. Moreover, effects that are typical of strong field ionization such as re-scattering, which was found to be important in [29], are not expected to play an important role in an attosecond streaking experiment discussed in this paper.

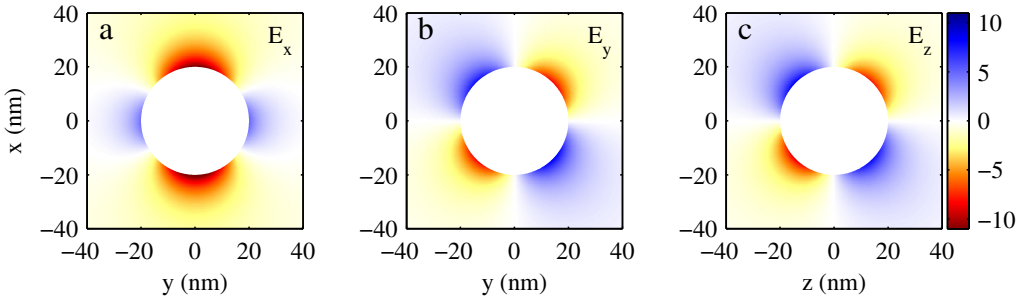

Figure 3. The x- (a) and the y-components (b) (xy-plane) and the z-component (c) (xz-plane) of the enhanced field in the vicinity of a 20 nm radius spherical silver particle under resonant excitation by a monochromatic wave at 362 nm at a phase where the field intensity enhancement is maximum. The values for the fields are normalized to the field amplitude of the incoming radiation.

3. Electron streaking by a plasmonic field

In our work we have considered resonant plasmonic fields of spherical silver particles. The fields on spherical metal particles are well described by Mie theory, an exact electrodynamic solution of Maxwell's equations for spherical particles based on a vector spherical harmonic expansion [2] and a frequency-dependent dielectric function [31]. In figure 3, the field intensity enhancement for a particle with a radius of 20 nm is plotted separately for the x- (a) and the y-components (b) in the xy-plane and for the z-component (c) in the xz-plane. The field in figure 3 closely resembles the field of a dipole at the center of the sphere. Higher order multipoles, although included, do not contribute significantly to the field of a particle of this size.

Similar to the work reported in [19], the attosecond streaking experiments are simulated by numerically integrating classical electron trajectories in the enhanced field of the nanoparticle under, in our case, resonant excitation, like the field that is shown in figure 3. The ionization step by the attosecond pulse is assumed to produce electrons instantaneously at t_i at a certain central energy W_0 and with a bandwidth that corresponds to a Fourier-limited pulse duration of a 300 as Gaussian pulse. This assumption is based on the fact that nowadays pulses with a duration down to 80 as exist [30]. Hence, even if smearing by the pulse duration is not a problem, it is crucial to verify that the streaking effect is not hidden within the bandwidth of the attosecond pulse. Evidently, this is a significant simplification of the photoionization process, which results in an idealized photoelectron spectrum that does not take into account the actual work function or internal band structure of the electrons in the metal. However, although a real spectrum is much more complicated, it usually contains distinguishable contributions of which the energy shifts can be tracked as a function of plasmon excitation in a streaking experiment. In this work we concentrate our analysis on the streaking dynamics and therefore the simplified ionization suffices. The electrons are born on the surface of the sphere from where the interaction with the field is calculated up to a point in time and space where the electron energy is constant. By varying the moment of release of the electrons within the electric field, the delay between the attosecond pulse and the incident resonant field is simulated. Here we take into account that the actual arrival time of the ionization pulse varies over the particle due to finite particle size. For a fixed delay τ between the ionization and the plasmon excitation pulse, the moment of

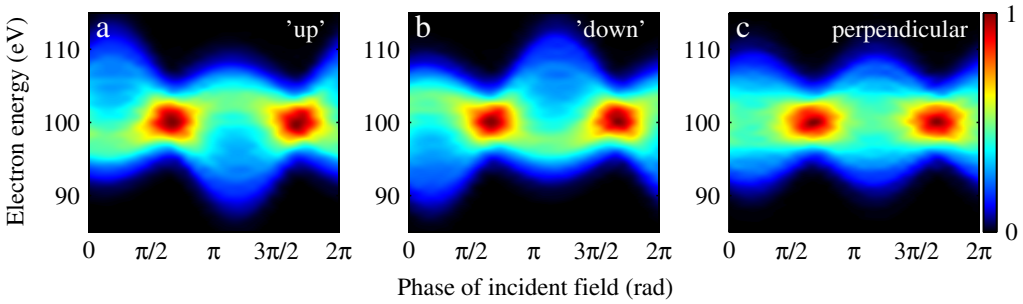

Figure 4. Attosecond streaking spectrograms from the enhanced field of a silver spherical particle with a radius of 20 nm from a Mie calculation resonantly driven by a monochromatic wave with a wavelength of 362 nm with an intensity of 10^{11} W cm^{-2}. Panels (a) and (b) are for electrons detected along the laser polarization in the opposite direction and panel (c) is for electrons detected perpendicular to the incident field polarization. In all cases, an acceptance angle of $\theta = \pm 40^{\circ}$ is used. Plotted in color scale is the normalized electron yield.

ionization is given by $t_i = \tau + z_{start}/c$ with z_{start} being the z-coordinate of the starting position of the trajectory. We assume that the attosecond ionization launches electrons in all directions from a uniform distribution on one-half of the sphere ($z < 0$). The other half of the sphere ($z > 0$) is assumed to be in the 'shadow', meaning that no electrons are produced. This is a good assumption when the wavelength of the attosecond pulse is small compared to the radius of the particle in which limit geometric optics applies. In any case, the results presented hardly depend on the geometrical assumption. The electric field at an arbitrary location is obtained by linear interpolation of the fields discussed in the previous section that are stored on a grid. Trajectories that return to and collide with the particle are terminated. The final energy W_f of the remaining trajectories is recorded. Since a continuous wave incident field is used in the Mie calculations, the vector potential of this continuous field is added to the momentum of the electron at the moment when the boundary of the box is reached. In this way the electron leaves the field adiabatically despite the fact that the incident field is a (continuous) plane wave.

3.1. Streaking in a plasmon field from Mie calculation

Figure 4 shows the result of a streaking simulation based on the field obtained with Mie theory for a spherical silver particle with a radius of 20 nm, resonantly driven by a monochromatic wave with a wavelength of 362 nm. The photoelectron spectrum as a function of the moment of release (ionization), which is here indicated as the phase of the incident field, is plotted for three different velocity (after interaction with the field) directions. Experimentally, it is possible to obtain these photoelectron spectra by using either an electron spectrometer with a narrow acceptance angle or resolving the angle of emission in an electron spectrometer with a larger acceptance angle and post-selecting the electrons of interest. Figures 4(a) and (b) show streaking spectrograms for electrons that fly out parallel to the incident field polarization, in the positive ('up') and negative ('down') x-direction, respectively. The plots in figure 4 are obtained by integrating over an acceptance angle of $\theta = \pm 40^{\circ}$. The results, however, do not depend strongly on the width of this angle. In stark contrast to the situation of laser field streaking, we observe a broadening of the electron energy distribution at certain delays, whereas in a laser field streaking

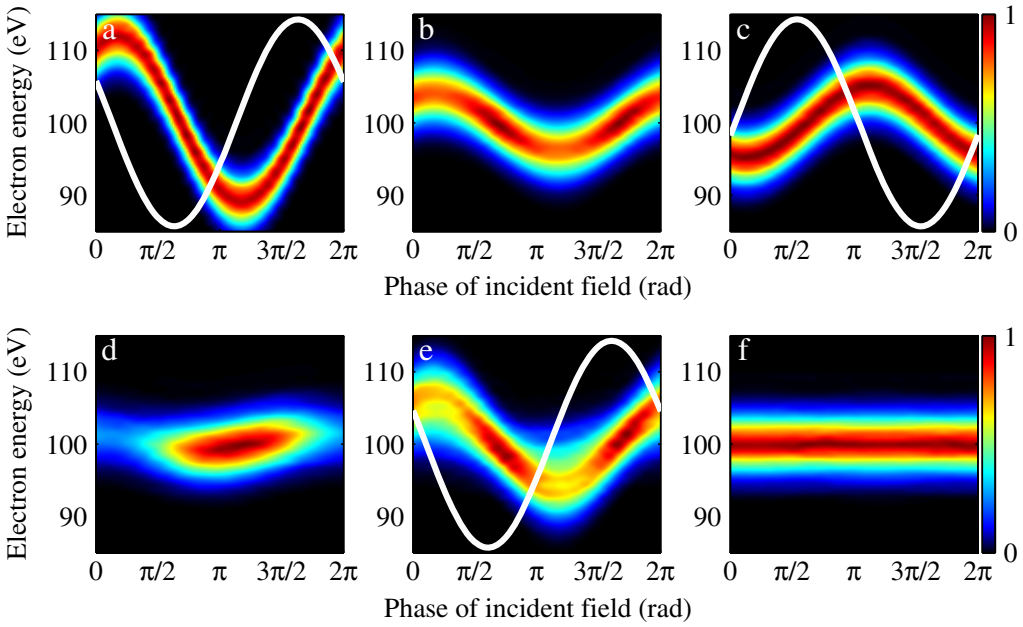

Figure 5. Streaking spectrogram from the same field as in figure 4 for electrons detected parallel (a)–(c) and perpendicular (d)–(f) with respect to the incident field polarization. The spectrograms show the results for electrons starting from different locations on the particle separately: for electrons that are born close to the pole of the sphere ($\theta \leqslant 5^\circ$) (a), (d), at 45° (b), (e) and close to the equator $85^\circ < \theta < 95^\circ$ (c), (f). The white curves in (a) and (c) show the time dependence of the x-component of the electric field where the electrons are born and in (e) it is the component that is perpendicular to the polarization. We note that results similar to (a)–(c) were recently reported in a paper by Borisov *et al* [20].

experiment an oscillating curve is obtained (figure 2). As in the case of streaking by a laser field, the streaking curve behavior is opposite for the 'up' (figure 4(a)) and the 'down' (figure 4(b)) directions. In figure 4(c), the result is plotted for electrons that fly out perpendicular to the incident field polarization. Because the system is cylindrically symmetric, all electron spectra are independent of the azimuthal angle ϕ of the velocity vector. The result in figure 4(c) is again different from what is observed in streaking by a laser field, where the electron spectrum is shifted down with a periodicity of half the optical cycle [22] (figure 2(a)). By contrast, figure 4(c) again shows a broadening of the electron kinetic energy distribution toward both higher and lower kinetic energy with a periodicity of half the optical cycle. The origin of the differences between what is observed here and what is found in laser field streaking experiments lies in the non-uniformity of the plasmon field and will now be discussed in more detail.

3.1.1. Angular and spatially resolved streaking curves.. In figure 5, streaking curves are plotted for electrons that are started from three specific locations on the particle: close to the pole ($\theta < 5^\circ$) (figures 5(a) and (d)), around the equator ($85^\circ < \theta < 95^\circ$) (figures 5(c) and (f)) and in between these two ($40^\circ < \theta < 50^\circ$) (figures 5(b) and (e)). For the three locations the streaking curve is plotted for electrons that are detected in the positive x-direction ('up') (figures 5(a)–(c))

and perpendicular to the laser polarization (figures 5(d)–(f)). The results presented in figure 4(a) can be seen as the result of the superposition of the streaking spectrograms in figures 5(a)–(c). The spectrogram in figure 4(c) corresponds to what is shown in figures 5(d)–(f) but in addition contains contributions from electrons originating from positions on the sphere with $90^\circ < \theta < 180^\circ$. We note that results similar to figures 5(a)–(c) were recently reported in the paper by Borisov *et al* [20].

The streaking curve in figure 5(a) is plotted along with the x-component of the enhanced field at the pole of the particle, demonstrating that the maximum shifts in the streaking curve occur close to the zero of the field. Note, however, that the oscillation of the enhanced field has a near-π phase difference with the incident field (not shown). Consequently, the oscillation in the streaking curve does not follow the vector potential of the incident field. The phase shift intrinsic to the plasmon resonance, which sweeps from 0 to π as the pump frequency is swept through, should therefore be directly observable when comparing plasmon streaking curves with reference streaking of the laser pulse.

The energy shifts that the electrons acquire are strongly dependent on the location on the nanoparticle where they are produced. The energy shift in figure 5(b) (birth at 45° with respect to the pole) is much smaller than in figure 5(a) (birth at the pole), whereas in figure 5(c) (birth at 90° with respect to the pole) it is slightly larger again. In figure 5(c) the x-component of the enhanced field (at $r = a\hat{y}$) is plotted on top of the electron spectrogram. The overlay of the enhanced field shows that the maximum energy shift coincides with the zeros of the field, similar to the situation in figure 5(a). It follows that the phase difference between the fields at the pole and the equator (see also figure 3(a)) is reflected in the two streaking curves in figures 5(a) and (c). This phase difference explains why both positive and negative energy shifts are seen simultaneously and result in the observed broadening of the electron energy distribution in figures 4(a) and (b). The smaller shift in figure 5(b) is because the x-component of the enhanced field experienced by electrons emitted from a point on the sphere around $\theta = 45^\circ$ is smaller than that at the pole ($\theta = 0^\circ$), as can be seen in figure 3(a). The y-component is maximum at this position, but for electrons with an initial velocity in the x-direction this will only cause a small (negative) shift. Generally, field components perpendicular to the electron velocity vector have a small effect, as is well known from standard laser field streaking. In attosecond laser field streaking, electrons that fly out perpendicularly to the laser polarization acquire a streaking contribution to their kinetic energy that is many times smaller than that for electrons flying out along the polarization (see figure 2). In a similar way, one can understand the streaking behavior that is found for electrons that are detected perpendicular to the incident field polarization in the plasmon streaking experiment (figures 5(d)–(f)). For these electrons the energy shift is maximum for the electrons that are emitted from a point on the sphere around $\theta = 45^\circ$ (figure 5(e)), whereas the energy shifts of electrons emitted close to the pole and the equator are much smaller. The behavior in figures 5(d)–(f) can be understood by considering the spatial dependence of the enhanced field in the components perpendicular to the laser polarization in figures 3(b) and (c), which is largest at the positions around $\theta = 45^\circ$ and 135°. The streaking curve in figure 4(c) contains contributions from both these positions ($\theta = 45^\circ$ and 135°), which yield oscillations that are exactly out of phase. Figure 4(c) therefore shows a superposition of two oscillations in antiphase. The 'residual' streaking effect in figures 5(b) and (d) that remains despite the largely out-of-phase nature of the field oscillations at the surface shows that interactions of electrons with the field further away from the surface are also important. Summarizing figures 4 and 5, we can conclude that in an attosecond streaking

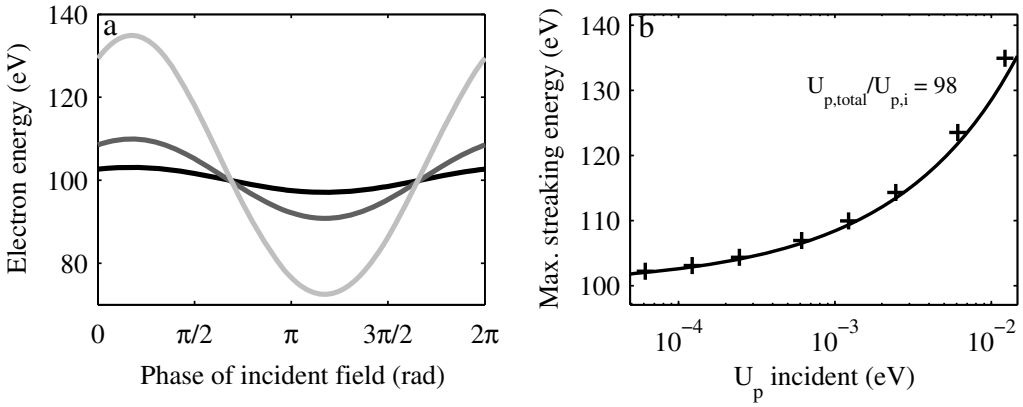

Figure 6. (a) The central photoelectron energy of electrons emitted from the pole of the particle detected along the laser polarization (figure 5(a)) for 10^{10} W cm^{-2} (black line), 10^{11} W cm^{-2} (dark gray line) and 10^{12} W cm^{-2} (gray line). (b) Maximum energy determined from curves as in (a) for eight different intensities plotted as a function of U_p of the incident field. The line is a fit to the data points using equation (2), from which a field intensity enhancement of 98 is determined.

experiment in localized fields, one can probe the different components of the plasmon field individually, provided one resolves the angular direction of the electrons.

3.1.2. Intensity dependence of the streaking results. To analyze further the character of the streaking observations just presented, the dependence on the intensity of the incident field is investigated for the case of emission in the positive x-direction from the pole of the particle (figure 4(a)). In figure 6, streaking curves are plotted for the incoming field intensities 10^{10} W cm^{-2} (black line), 10^{11} W cm^{-2} (dark gray line) and 10^{12} W cm^{-2} (light gray line). For these curves the photoelectron spectrum at each delay is fitted to a Gaussian from which the peak position is determined. In figure 6(b) the maximum energy (for all delays) is plotted as a function of U_p of the incident field. The 'plus' symbols are the result of eight separate streaking simulations and the line is a fit based on equation (4), in which the effective U_p is used as the fitting parameter. The value for U_p determined in the fit gives a factor of 98 for the field intensity enhancement, i.e. the enhancement of $|E|^2$. Clearly, the fit describes the intensity dependence rather well and the value for the field intensity enhancement is not far from the value of 120 at the surface of the sphere close to the pole. Attosecond streaking experiments could therefore allow us to estimate field intensity enhancements directly when the streaking regime is known. Deviations are the result of not completely fulfilling the condition of an adiabatic exit of the field. In order to determine how far attosecond streaking will operate in any one of the three regimes sketched in figure 1, we now proceed to discuss streaking as a function of the initial energy of the electron.

3.1.3. Transition from the adiabatic to the instantaneous regime. In figure 1, three limiting situations for attosecond streaking are sketched. When streaking in a free laser pulse, the electron stays in the field for the whole pulse duration. The highly localized plasmon fields can give rise to two distinct regimes. If the field is extended over a scale comparable to the travel

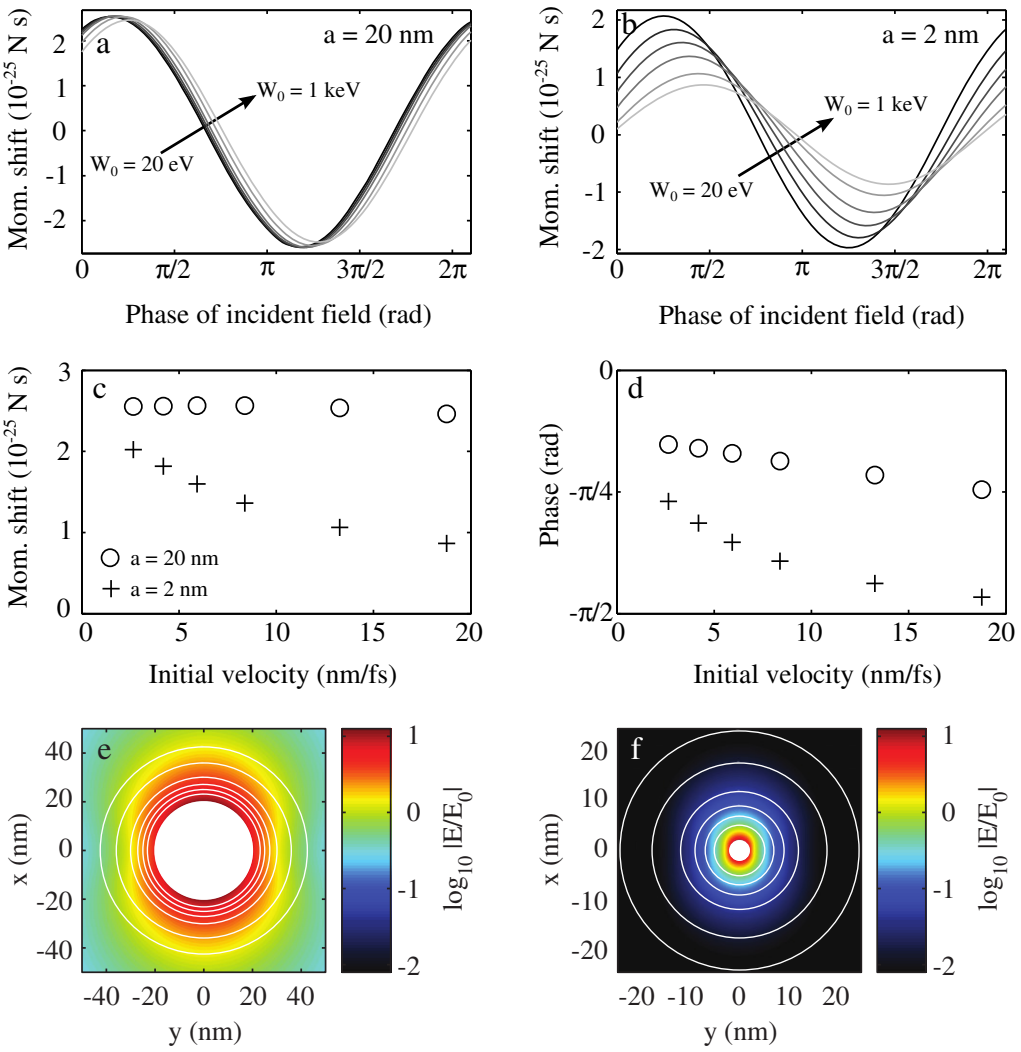

Figure 7. Electron momentum shift for a 20 nm (a) and a 2 nm (b) particle for six starting energies W_0 between 20 eV and 1 keV. The amplitude (c) and phase (b) of these oscillations are plotted as a function of the initial velocity of the electron for 20 nm (o) and 2 nm (+) particles. Panels (e) and (f) show contour plots of the field enhancement around both particles using the same logarithmic color scale. While field enhancements right on the sphere surface are almost identical, the spatial extent of the field for the small particle is much smaller. For comparison with the criterion for adiabaticity, we plot circles at distances $2v_0/\omega_0$, i.e. the distance an electron travels in a single optical cycle, away from the sphere edge, for kinetic energies 20, 50, 100, 200, 500 and 1000 eV.

distance of the electron during the many optical cycles that the plasmon field oscillates, the electron is said to leave the field adiabatically ($2\pi v_0/\omega \ll r_0 \ll v_0 t_p$). In contrast, the electron exits instantaneously if the field extent is so small that the electron leaves the field within a fraction of an optical cycle ($r_0 \ll 2\pi v_0/\omega$). The streaking behavior in the last case is very different from the other two. A particularly striking difference is the different relative phase

between the streaking oscillation and the streaking field, which is $\pi/2$ in the adiabatic regime but 0 in the instantaneous regime. The results presented in figures 4–6 indicate that for a particle with a radius of 20 nm, and an initial electron energy of 100 eV the situation is best described by the adiabatic regime, since it shows a phase difference with the field of $\pi/2$ (figure 5(a)) and the streaking curve is well described by equation (4) (figure 6). In figure 7(a), results are presented for the same particle size but for different starting energies. The momentum shift of the electrons is plotted as a function of the phase of the incident field at the moment the electron is born for six starting energies in the range between 20 eV and 1 keV. Again the electrons from the pole of the sphere detected parallel to the laser polarization in the positive direction are selected. The curves almost lie on top of each other, which is expected for a situation where the electron moves out of an oscillating field adiabatically. Indeed, in the adiabatic regime, the momentum shift should only depend on the properties of the field and should be independent of the initial velocity. The situation is clearly very different for a particle with a radius of 2 nm, which is shown in figure 7(b). The phase and amplitude of the oscillation in the momentum shift then significantly change with the starting energy W_0. For small initial velocities the momentum shift approximates the momentum shift observed for the larger particles, but for larger initial velocities a substantial drop in the momentum shift is observed because the particle exits the plasmonic field before it turns off. In other words, the dependence on the starting energy W_0 is the result of moving from the regime of an adiabatic exit (small initial velocity) to an instantaneous exit (high initial velocity). The phase shift is only approximately $\pi/4$, rather than $\pi/2$, because the asymptotic conditions for neither regime are met at either of the extremes in the W_0 range. The transition between the two regimes is gradual both in phase and in amplitude (see figures 7(c) and (d)). In the asymptotic limits (small radius, large initial velocity and large radius, small initial velocity), the streaking behavior is well understood and the phase and amplitude are related to the phase and amplitude of the field in a simple way. In the transition regime the streaking depends not only on the phase and amplitude of the enhanced field, but also on its geometrical extension.

3.2. Streaking in a plasmon field from a finite-difference time-domain simulation

Simulations that are based on the Mie theory are very convenient, since they allow one to describe the field in an analytical form. However, when more complicated, non-spherical nano-structures are used, it becomes necessary to resort to numerical methods, such as FDTD. Due to the intrinsically pulsed nature of plasmon streaking, the FDTD method [32] is an especially appropriate tool to simulate complex structures. A frequent problem with numerical methods that use non-conformal gridding of plasmonic objects, such as the standard Yee grid used in FDTD solvers, is the occurrence of artifacts. Due to staircase discretization on a rectangular grid, the boundary conditions that require continuity of $E_{\|}$ and $H_{\|}$ are not accurately represented exactly at the surface of the plasmonic object. As a consequence, in many reported calculations, artifacts appear that are visible as highly intense hot spots of very high $|E|^2$ at the object surface that, furthermore, represent strongly polarized fields with locally incorrect field orientation. Although the volume containing artifacts of just one grid cell layer shrinks with grid refinement, the hot spot artifacts commonly remain high in strength at any level of grid refinement. Since such hot spots could significantly alter the predictions, we explicitly benchmark that FDTD is suited for predicting streaking measurements. In order to assess the suitability of FDTD for predicting the results of streaking measurements, a comparison was

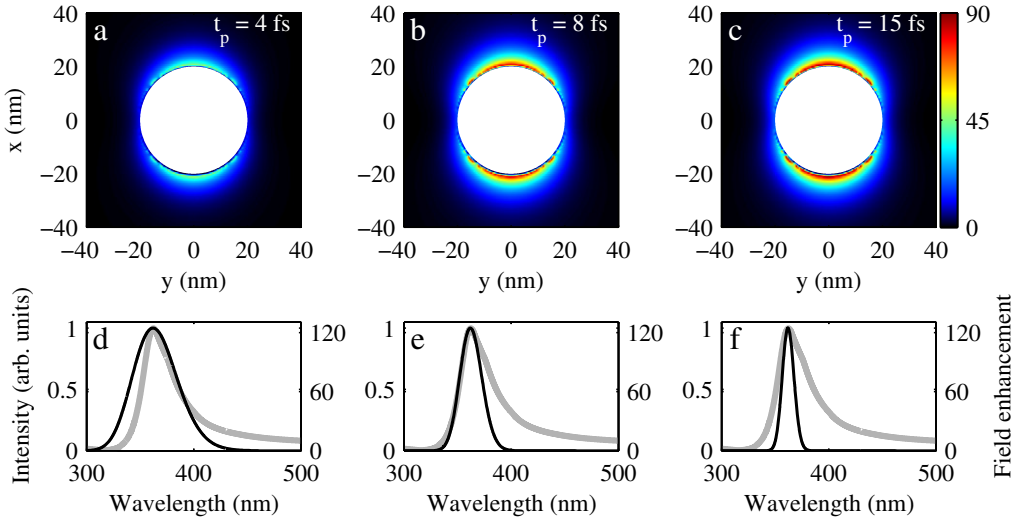

Figure 8. Maximum field intensity enhancement in the xy-plane calculated by FDTD for a 20 nm spherical silver particle excited by a resonant 362 nm pulse of (a) 4 fs, (b) 8 fs and (c) 15 fs. The spectra of the incident field (black lines) of 4 fs (d), 8 fs (e) and 15 fs (f) are compared with the wavelength dependence of the field intensity enhancement from a Mie calculation (gray lines).

made between the aforementioned results according to Mie theory and the numerical results obtained by means of FDTD (Lumerical FDTD Solutions v7.0). For the FDTD simulations, we have used a grid of $1 \times 1 \times 1\ \mu\text{m}^3$ with a minimum step size of 0.5 nm and perfectly matched layer (PML) absorbing boundaries. We have applied symmetry rules in two dimensions. An extended analytical model was used for the optical constants to match the constants in the Mie calculations as closely as possible. However, discrepancies remain resulting in deviations in the field enhancement factor between the Mie calculation and the FDTD result. Optical constants in FDTD have to be represented by an auxiliary time-dependent differential equation for polarization in the matter, so that only the Drude and Lorentz descriptions can be simulated. This restriction will result in deviations from the tabulated data, and hence in the fields.

Figures 8(a)–(c) show a reduction in the field enhancement for a 20 nm silver particle excited by a 4 fs full-width at half-maximum pulse, as compared to a 15 fs pulse, as the pulse bandwidth exceeds the plasmon resonance linewidth (spectra in figures 8(d)–(e)). Compared to continuous wave calculations, a 30% reduction in field strength remains even for the longest 15 fs pulse. That the dispersive character of the collective plasmon resonance is important for determining the local response in ultrashort-pulse experiments was already appreciated in [33].

Figure 9 shows the simulated streaking spectrograms for the FDTD fields in figures 8(a)–(c) for electrons detected along the polarization in the positive x-direction (i.e. the same conditions as in the Mie calculation shown in figure 4(a)). The zero of the delay axis was chosen such that the attosecond pulse overlaps with the center of the incoming pulse. The maximum streaking amplitudes are reached a few fs after the center of the incoming pulse has reached the particle. The first observation in figure 9 is that, for the shortest pulse duration (figure 9(b)), the energy shifts are smaller than those for the two longer pulses (figures 9(d)–(f)), assuming identical peak field strengths of the driving field. The smaller streaking effect in

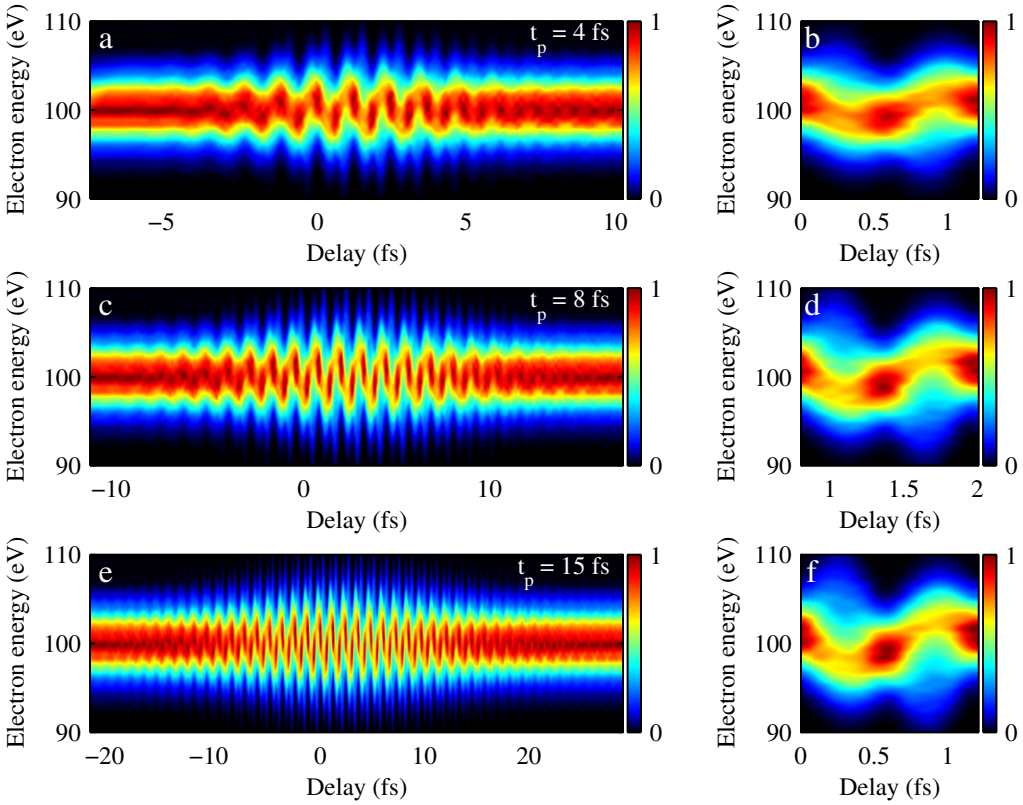

Figure 9. Attosecond streaking spectrograms for electrons detected along the laser polarization in the positive x-direction within an acceptance angle of $\theta \pm 40^\circ$. The simulations are based on the FDTD fields from figure 8 for an incident intensity of $10^{11}\,\mathrm{W\,cm^{-2}}$. Panels (a), (c) and (d) show delays covering the entire pulse duration and in (e), (f) and (g) a zoom-in over a single cycle of the field is given. The zero on the delay axis marks the center of the incoming pulse.

figure 9(b) is a direct consequence of the aforementioned finite bandwidth of the resonance (figures 8(d)–(f)). The reduced streaking effect shows that in an actual experiment one might not necessarily opt for the shortest pulse durations available. The importance of choosing longer pulse durations tuned to the resonance linewidth will be especially important for studying plasmon fields in coupled systems. For instance, it was recently predicted that strong local excitations can be realized using narrow Fano resonances that result from coherent coupling between bright and dark modes in plasmonic molecules, a phenomenon called plasmon-induced transparency [34].

Another observation is that even after the incident field has vanished ($\tau > 10\,\mathrm{fs}$), oscillations resulting from the finite lifetime of the plasmon are observed. From this asymmetry in the streaking spectrogram the dephasing time of the plasmon can be extracted. These spectrograms would allow for a complete characterization of the incident and plasmon fields including the *carrier envelope phase* (CEP) of both fields if at the same time a reference streaking spectrogram is measured that depends on the incident field rather than the plasmon field.

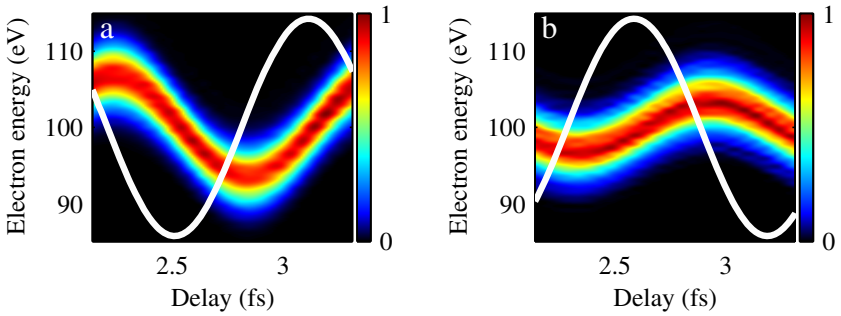

Figure 10. Streaking spectrogram for the same situation as in figure 9(b) for electrons that started close to the pole of the particle (a) and around the equator (b). The white curves show the time dependence of the x-component of the electric fields at the locations where the electrons are born. The delay range is chosen such that a direct comparison can be made to figures 5(a) and (c).

To compare the results from the FDTD fields with the results obtained with the field from a Mie calculation, the streaking spectrogram from figure 9(b) is separated into the contributions originating from the pole (figure 10(a)) and the equator (figure 10(b)) of the particle as was done before in figure 5. The x-component of the enhanced field at the respective locations is plotted on top of the streaking spectrograms. The maximum shifts in energy coincide with the zeros of the field, as was the case in previous calculations based on a field from a Mie solution. The amplitude of the oscillation is slightly smaller than that in the Mie results, which is attributed to the fact that the field intensity enhancement in the FDTD fields is about 30% smaller than in the Mie calculation.

4. Application to experiments

So far we have considered the electron streaking dynamics in general. In this section, we would like to discuss a number of key issues related to the practical implementation of attosecond plasmon experiments.

The situation that most closely resembles that in our simulations would be an experiment in which metallic nanoparticles can be injected into a photoelectron spectrometer by a gas jet. The experimental conditions would closely resemble those of traditional attosecond streaking experiments [15]. The main additional complexity is the need for the incident field to match the resonance of the particles under investigation. The calculations presented here suggest that the second harmonic of a Ti:sapphire laser could be used as the incident field. Besides homogeneous spherical particles, the so-called core–shell and ellipsoidal particles will be of interest as well. In such particles, the resonance can be shifted toward longer wavelengths and potentially a higher field intensity enhancement can be achieved.

Attosecond streaking studies of plasmonic structures on a surface would be a much more general way of studying plasmon fields. Such structures are produced by either nanofabrication methods or deposition of nanoparticles. Attosecond streaking experiments on surface emitted photoelectrons have already been performed [35]. Simulating such an experiment would require extending the models to include the surface. Including structures other than spheres requires numerical techniques such as FDTD, discrete dipole approximation (DDA) or the use of techniques based on surface integral methods that can conformally grid the metal surfaces,

thereby avoiding the staircasing discretization issues of Cartesian gridding conventionally used in, e.g., FDTD [36].

In this study, we have focused on silver particles because they have the largest optical response. Besides silver, also aluminum, copper and gold nanoparticles show significant field enhancements [37]. For gas phase experiments, however, we envision that one would use colloidal particles, in which case only silver and gold particles are readily available. For lithographically defined structures, the geometry of the structure becomes at least as important as the material. For example, in a dimer gap the field enhancement can be much higher than that for any single particle even if the dimer is made of a poorer metal.

A crucial parameter in an experiment is the electron yield, which will be dependent on the density of particles, the number of photons per area, repetition rate and detection efficiency. In [19], count rates of about 1 electron per second were calculated as being possible, using a 10 kHz source of isolated attosecond pulses, with 10^5 photons per shot. Using novel schemes for the generation of intense isolated attosecond pulses, such as ionization gating [38], we may anticipate increases in the intensity of isolated attosecond pulses of at least two orders of magnitude, leading to the situation where the experiments can be confidently attempted.

5. Conclusions and outlook

In this paper, we have investigated attosecond streaking spectroscopy as a tool for the characterization of plasmon fields. A general method for simulating such experiments is presented based on Mie theory and FDTD simulations. Analytical theories like Mie theory exist only for a limited number of cases. The comparison between the results based on fields from a Mie calculation and those based on FDTD fields shows that there is good agreement. The good agreement indicates that the method based on FDTD is reliable despite the numerical artifacts that occur at the interface of the metal particle.

The key difference between plasmon streaking and conventional streaking is that the conventional assumption that the pulse dies out before the electron has left the spatial extent of the field is violated. From our simulations, we conclude that this violation does not prevent one resolving the oscillations of the plasmon field. In most practical situations, the electron moves out of the field adiabatically allowing one to resolve the phase and the amplitude from localized fields. These experiments would enable us therefore to measure independently both the field intensity enhancement and the dephasing time, which can form a strong test for existing models. Moreover, with attosecond streaking one can resolve the absolute phase (CEP) of the field rather than only relative phases that are resolved in techniques based on interferometry with long pulses (e.g. FROG).

We have shown that the exit of the electron from the field is no longer adiabatic for sufficiently high starting velocities and/or sufficiently small field extensions. The departure from adiabatic conditions is reflected in changes of both the phase and the amplitude of the streaking curves. Ultimately, one would arrive at the instantaneous limit proposed by Stockman *et al* [16]. However, in practice, we expect that experiments will at best reach midway into the transition between the adiabatic and the instantaneous. In the transition between the adiabatic and the instantaneous regime, the phase and amplitude of the streaking curves are no longer related to the phase and amplitude of the field in a straightforward manner. Furthermore, if one were to scan the incident wavelength over the plasmon resonance wavelength, attosecond streaking would reveal the associated phase-flip of the plasmon response from 0 to π.

A second difference compared with conventional attosecond streaking beyond the limited spatial range of the field is the large spatial and vectorial non-uniformity of the field over the surface of the plasmon object. In agreement with the recent paper by Borisov *et al* [20], our calculations show the profound effect of such non-uniformities on streaking spectrograms. The streaking spectrograms for localized fields contain distinct oscillatory contributions of different amplitudes and phase offset oscillations on top of each other originating from different positions on the particle, instead of consisting of a single oscillation as in the case of streaking by a laser field. Obviously, spatially resolving these contributions would be desirable but will be extremely challenging, even with a PEEM instrument [16, 39]. Interestingly, by resolving the angle of emission of the electron one can probe the different vector components of the localized fields individually.

Acknowledgments

This work is part of the research program 'Stichting voor Fundamenteel Onderzoek der Materie (FOM)', which is financially supported by the Nederlandse organisatie voor Wetenschappelijk Onderzoek (NWO). AFK acknowledges support through a VIDI fellowship funded by the NWO.

References

[1] Raether H 1988 *Surface Plasmons on Smooth and Rough Surfaces and on Grattings* (Berlin: Springer)
[2] Mie G 1908 Beiträge zur optik trüber medien, speziell kolloidaler metallösungen *Ann. Phys.* **330** 377–445
[3] Barnes W L, Dereux A and Ebbesen T W 2003 Surface plasmon subwavelength optics *Nature* **424** 824–30
[4] Fleischmann M, Hendra P J and McQuillan A J 1974 Raman spectra of pyridine adsorbed at a silver electrode *Chem. Phys. Lett.* **26** 163–6
[5] Nie S M and Emery S R 1997 Probing single molecules and single nanoparticles by surface-enhanced Raman scattering *Science* **275** 1102–6
[6] McMahon J M, Gray S K and Schatz G C 2009 Nonlocal optical response of metal nanostructures with arbitrary shape *Phys. Rev. Lett.* **103** 097403
[7] Zuloaga J, Prodan E and Nordlander P 2009 Quantum description of the plasmon resonances of a nanoparticle dimer *Nano Lett.* **9** 887–91
[8] García de Abajo F J 2008 Nonlocal effects in the plasmons of strongly interacting nanoparticles, dimers and waveguides *J. Phys. Chem.* C **112** 17983–7
[9] Lamprecht B, Leitner A and Aussenegg F R 1997 Femtosecond decay-time measurement of electron–plasma oscillation in nanolithographically designed silver particles *Appl. Phys.* B **64** 269–72
[10] Lamprecht B, Leitner A and Aussenegg F R 1999 SHg studies of plasmon dephasing in nanoparticles *Appl. Phys.* B **68** 419–23
[11] Lamprecht B, Krenn J R, Leitner A and Aussenegg F R 1999 Resonant and off-resonant light-driven plasmons in metal nanoparticles studied by femtosecond-resolution third-harmonic generation *Phys. Rev. Lett.* **83** 4421–4
[12] Anderson A, Deryckx K S, Xu X G, Steinmeyer G and Raschke M B 2010 Few-femtosecond plasmon dephasing of a single metallic nanostructure from optical response function reconstruction by interferometric frequency resolved optical gating *Nano Lett.* **10** 2519–24
[13] Zentgraf T, Christ A, Kuhl J and Giessen H 2004 Tailoring the ultrafast dephasing of quasiparticles in metallic photonic crystals *Phys. Rev. Lett.* **93** 243901
[14] Stietz F, Bosbach J, Wenzel T, Vartanyan T, Goldmann A and Träger F 2000 Decay times of surface plasmon excitation in metal nanoparticles by persistent spectral hole burning *Phys. Rev. Lett.* **84** 5644–7

[15] Goulielmakis E *et al* 2004 Direct measurement of light waves *Science* **305** 1267–9
[16] Stockman M I, Kling M F, Kleineberg U and Krausz F 2007 Attosecond nanoplasmonic-field microscope *Nature Photon.* **1** 539–44
[17] Pfeifer T, Abel M J, Nagel P M, Jullien A, Loh Z H, Bell M J, Neumark D M and Leone S R 2008 Time-resolved spectroscopy of attosecond quantum dynamics *Chem. Phys. Lett.* **463** 11–24
[18] Skopalová E, Lei D Y, Witting T, Arrell C, Frank F, Sonnefraud Y, Maier S A, Tisch J W G and Marangos J P 2011 Numerical simulation of attosecond nanoplasmonic streaking *New J. Phys.* **13** 083003
[19] Süßmann F and Kling M F 2011 Attosecond nanoplasmonic streaking of localized fields near metal nanospheres *Phys. Rev.* B **84** 121406
[20] Borisov A G, Echenique P M and Kazansky A K 2012 Attostreaking with metallic nano-objects *New J. Phys.* **14** 023036
[21] Itatani J, Quere F, Yudin G L, Ivanov M Y, Krausz F and Corkum P B 2002 Attosecond streak camera *Phys. Rev. Lett.* **88** 173903
[22] Drescher M, Hentschel M, Kienberger R, Tempea G, Spielmann C, Reider G A, Corkum P B and Krausz F 2001 X-ray pulses approaching the attosecond frontier *Science* **291** 1923–7
[23] Lewenstein M and L'Huillier A 2008 Principles of single atom physics: high-order harmonic generation, above-threshold ionization and non-sequential ionization *Strong Field Laser Physics* ed T Brabec (*Springer Series in Optical Sciences*) (Berlin: Springer) pp 147–83
[24] Kupersztych J, Monchicourt P and Raynaud M 2001 Ponderomotive acceleration of photoelectrons in surface-plasmon-assisted multiphoton photoelectric emission *Phys. Rev. Lett.* **86** 5180–3
[25] Irvine S E, Dechant A and Elezzabi A Y 2004 Generation of 0.4-keV femtosecond electron pulses using impulsively excited surface plasmons *Phys. Rev. Lett.* **93** 184801
[26] Irvine S E and Elezzabi A Y 2006 Surface-plasmon-based electron acceleration *Phys. Rev.* A **73** 013815
[27] Irvine S E, Dombi P, Farkas G and Elezzabi A Y 2006 Influence of the carrier-envelope phase of few-cycle pulses on ponderomotive surface-plasmon electron acceleration *Phys. Rev. Lett.* **97** 146801
[28] Dombi P *et al* 2010 Observation of few-cycle, strong-field phenomena in surface plasmon fields *Opt. Express* **18** 24206–12
[29] Zherebtsov S *et al* 2011 Controlled near-field enhanced electron acceleration from dielectric nanospheres with intense few-cycle laser fields *Nature Phys.* **7** 656–62
[30] Goulielmakis E *et al* 2008 Single-cycle nonlinear optics *Science* **320** 1614-7
[31] Palik E D (ed) 1985 *Handbook of Optical Constants of Solids* (New York: Academic)
[32] Taflove A and Hagness S C 2005 *Computational Electrodynamics: The Finite-Difference Time-Domain Method* 3rd edn (Boston, MA: Artech House Publishers)
[33] Merschdorf M, Kennerknecht C and Pfeiffer W 2004 Collective and single-particle dynamics in time-resolved two-photon photoemission *Phys. Rev.* B **70** 193401
[34] Zhang S, Genov D A, Wang Y, Liu M and Zhang X 2008 Plasmon-induced transparency in metamaterials *Phys. Rev. Lett.* **101** 047401
[35] Cavalieri A L *et al* 2007 Attosecond spectroscopy in condensed matter *Nature* **449** 1029–32
[36] Kern A M and Martin O J F 2009 Surface integral formulation for 3D simulations of plasmonic and high permittivity nanostructures *J. Opt. Soc. Am.* A **26** 732–40
[37] Tanabe K 2008 Field enhancement around metal nanoparticles and nanoshells: a systematic investigation *J. Phys. Chem.* C **112** 15721–8
[38] Ferrari F, Calegari F, Lucchini M, Vozzi C, Stagira S, Sansone G and Nisoli M 2010 High-energy isolated attosecond pulses generated by above-saturation few-cycle fields *Nature Photon.* **4** 875–9
[39] Mikkelsen A *et al* 2009 Photoemission electron microscopy using extreme ultraviolet attosecond pulse trains *Rev. Sci. Instrum.* **80** 123703